Ionics (2018) 24:3967–3973
https://doi.org/10.1007/s11581-018-2552-0

ORIGINAL PAPER

# One-step and low-temperature synthesis of $CoMoO_4$ nanowire arrays on Ni foam for asymmetric supercapacitors

Jing Wang[1] · Jiang Chang[1] · Lu Wang[2] · Jian Hao[3]

Received: 2 February 2018 / Revised: 12 March 2018 / Accepted: 1 April 2018 / Published online: 18 May 2018


## Abstract

Herein, we report a rational synthesis of branched $CoMoO_4$ nanowire arrays (NWAs) with remarkable supercapacitor performance on Ni foam via facile low-temperature (95 °C) one-step hydrothermal method. The $CoMoO_4$ NWAs yielded high specific capacitance, rate performance, and cycling stability. Moreover, the asymmetric supercapacitor device was assembled by virtue of the as-prepared $CoMoO_4$ NWAs as positive electrode and the activated carbon (AC) as negative electrode. This asymmetric supercapacitor device exhibits a maximum voltage of 1.6 V and high energy density (46.7 Wh $kg^{-1}$ at a power density of 800 W $kg^{-1}$) as well as power density (8000 W $kg^{-1}$ at 26.7 Wh $kg^{-1}$). Such outstanding electrochemical performance implied the as-prepared $CoMoO_4$ NWA electrode will be a prospective candidate for supercapacitors.

**Keywords** One-step · Low-temperature synthesis · $CoMoO_4$ nanowire arrays · Asymmetric supercapacitors · Energy storage

## Introduction

High energy storage is an urgently solved problem since the growing demand of daily life. Supercapacitors (SCs) are one of the most promising energy devices for their high power density, fast charge-discharge property, long cycle life, light weight, and environmental protection [1–4]. However, the energy density of the SCs is unsatisfactory and hindering their practical applications [5–8]. The energy density ($E$) can be improved by enhancing the specific capacitance ($C$) and the potential window ($V$) according to the energy density equation ($E = 1/2\, CV^2$) [9]. Therefore, an effective method is to fabricate the asymmetric supercapacitors (ASC), which can make full use of the different potential windows of the two electrodes to provide a maximum operation voltage, accordingly resulting in a greatly enhanced specific capacitance [10, 11].

Electrode materials and their structures act as a critical role in the electrochemical performance [12–16]. Transition metal oxides are promising electrode materials for SCs because of their multiple oxidation states and high energy density. Nanostructured transition metal oxides have been approved to be promising candidates for assembling SCs electrodes because of their largely enhanced or modified electrochemical performance [17–21]. Among those metal oxides, binary metal oxides show higher performances than single component oxides due to their feasible oxidation states and high electrical conductivity, which seem to be the potential materials for high performance. $CoMoO_4$ has been considered to be promising metal oxide electrode materials due to its simple synthesis, low cost, outstanding conductivity, and superior rate capability [16, 22]. Therefore, the molybdenum and cobalt binary oxide with unique morphologies and enhanced capacitive behavior have attracted great research interests. To improve supercapacitive behavior, it is crucial to enhance the kinetics of ion and electron transport inside the electrodes and at the electrode/electrolyte interface. An effective way is to fabricate active material with one-dimensional structures, because they can provide short diffusion path lengths for the ions, leading to high charge/discharge rates.

**Electronic supplementary material** The online version of this article (https://doi.org/10.1007/s11581-018-2552-0) contains supplementary material, which is available to authorized users.

✉ Jing Wang
wangwangmayong@126.com

1 School of Light Industry, Harbin University of Commerce, Harbin 150028, People's Republic of China

2 College of Aerospace and Civil Engineering, Harbin Engineering University, Harbin 150001, People's Republic of China

3 State Key Laboratory of High-efficiency Utilization of Coal and Green Chemical Engineering, Ningxia University, Ningxia 750021, People's Republic of China

In this contribution, we report a simple one-step hydrothermal method to prepare $CoMoO_4$ nanowire array (NWAs) electrodes under low temperature 95 °C. These $CoMoO_4$ NWAs directly grew on Ni foam with superior electrochemical properties. The asymmetric SCs were assembled by $CoMoO_4$ NWAs as the positive and AC as the negative. This ACS can provide a maximum of 46.7 Wh $kg^{-1}$ energy density (at the current density of 1 A $g^{-1}$ with power density 800 W $kg^{-1}$) and a maximum of 8000 W $kg^{-1}$ power density (at the current density of 10 A $g^{-1}$ with energy density of 26.7 Wh $kg^{-1}$) with an operating potential of 1.6 V.

## Experiment

### Synthesis of the $CoMoO_4$ NWAs

The $CoMoO_4$ NWAs were grown directly on Ni foam substrate by a facile one-step and low-temperature hydrothermal method. Firstly, 5 mM $Co(NO_3)_2$•$6H_2O$ and 5 mM $Na_2MoO_4$•$7H_2O$ were dissolved in 60 mL deionized water under magnetic stirring for 2 h. Secondly, the mixed solution was transferred into a 100-mL Teflon-lined stainless steel autoclave with a piece of pretreated Ni foam (the area 1 × 1 $cm^2$). The autoclave was sealed and maintained at 95 °C for 4 h and then cooled to room temperature. Subsequently, the products were collected and washed with distilled water and ethanol for several times. Finally, the $CoMoO_4$ products were obtained by drying at 60 °C for 10 h in the air.

The active carbon (AC) was used as the negative electrodes for ASC. It was prepared by mixing AC (85 wt%) with carbon black (10 wt%) and polyvinylidenefluoride (PVDF, 5 wt%). A small amount of N-methylpyrrolidone (NMP) was then added to form a homogeneous mixture. The resulting mixture was coated onto the Ni foam and dried at 80 °C for 12 h.

### Materials characterizations

Scanning electron microscopy (SEM, Hitachi S-4800) and transmission electron microscopy (TEM, JEOL JEM-2010) were employed for the characterization of the microstructure of the as-prepared materials. X-ray diffraction (XRD, Rigaku D/max-rB, Cu K$\alpha$ radiation, $\lambda = 0.1542$ nm, 40 kV, 100 mA) was used for the phase structures.

### Electrochemical measurements

Electrochemical tests were conducted by an electrochemical workstation (CHI 660D, Shanghai, China) using a three-electrode mode in 2 M KOH aqueous solution within the potential window of − 0.2 to 0.6 V. The mass of nickel foam (1 $cm^2$ area) is 0.1071 g. The nickel foam supported $CoMoO_4$ (the mass of nickel foam and $CoMoO_4$ are 0.1095 g). Therefore, the nickel foam supported pristine $CoMoO_4$ (mass 2.4 mg). The nickel foam supported $CoMoO_4$ acted directly as the working electrodes. A platinum electrode and a saturated calomel electrode (SCE) served as the counter electrode and the reference electrode, respectively. Electrochemical impedance spectroscopy (EIS) measurements were carried out by applying an alternating voltage with 5 mV amplitude in a frequency range from 0.1 Hz to 100 kHz at open circuit potential. The specific capacitance, energy density, and power density were calculated from the following equations:

$$C_s = it/mV \tag{1}$$

$$E = 0.5C_sV^2/3.6 \tag{2}$$

$$P = 3600E/t \tag{3}$$

$C_s$ (F $g^{-1}$) is the specific capacitance, $i$ (A) is the constant discharge current, $t$ (s) is the discharge time, $V$ (V) is the potential drop, $m$ (g) is the mass of the active materials, $E$ (Wh $kg^{-1}$) is the energy density, and $P$ (W $kg^{-1}$) is the power density.

### Preparation and characterization of the asymmetric supercapacitor

The ASC ($CoMoO_4$//AC) was assembled by using $CoMoO_4$ NWAs as positive electrode, and AC as negative electrode. Each electrode had the area 1 $cm^2$. The electrochemical performance of the ASC was tested by an electrochemical workstation (CHI 660D, Shanghai, China) using a two-electrode mode.

The mass of positive and negative is different. For the ASC, the charge balance contains the relationship q + = $q^-$, where q + and $q^-$ respectively reflect the charge in positive electrode and negative electrode. The q of each electrode depends on the specific capacitance ($Cs$), the potential range of the charge-discharge tests ($\Delta V$), and the mass of the electrode materials according to the following equation:

$$q = Cs \times \Delta V \times m \tag{4}$$

when q + = q-, the masses of the positive electrode ($m_+$) and negative electrode ($m_-$) will follow the equation:

$$m_+/m_- = C_- \times \Delta V_/ C_+ \times \Delta V_+ \tag{5}$$

The specific capacitances of the AC and $CoMoO_4$ NAWs are 125 and 950 F $g^{-1}$ at the same current density 1 A $g^{-1}$, respectively. On the basis of the specific capacitance values and the potential windows for the AC and $CoMoO_4$ electrodes, the optimal mass ration should be $m_+/m_- \approx 1/3$ according to Eq. (5) for assembling the ASC device. Herein, the masses of the AC and $CoMoO_4$ electrodes are 7.2 and 2.4 mg, respectively.

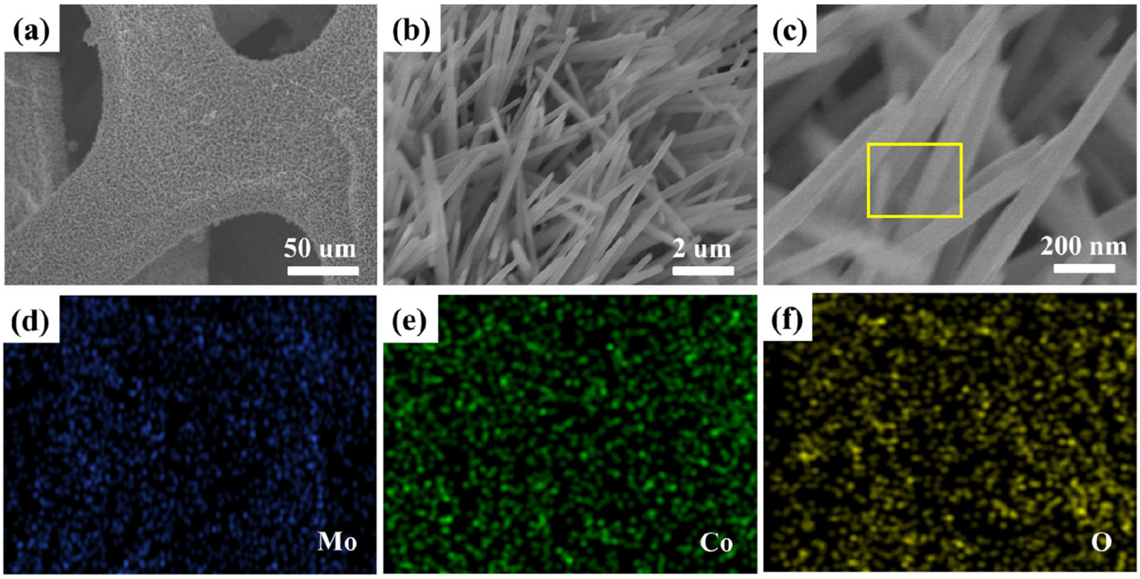


**Fig. 1** **a**–**c** SEM images of $CoMoO_4$ NWAs at different magnifications. **d**–**f** SEM mapping images of Mo, O, and O elements, respectively

## Results and discussion

Figure 1a displays the low magnification SEM image of the as-prepared $CoMoO_4$ products grown on Ni foam, indicating that the Ni substrate was fully covered. Figure 1b indicates the middle magnification SEM image of the obtained products. It can be found that some nanowires (NWAs) were arrayed and interconnected with each other. Figure 1c demonstrates the high magnification SEM image of the $CoMoO_4$ NWAs with the diameter about 100 nm. Taking the yellow section for SEM mapping tests, the results confirm the existence of Mo, Co, and O elements (as shown in Fig. 1d–f).

Further taking the yellow section for EDS analysis (Fig. 2a), Mo, Co, and O elements can be detected, which is consistent with the SEM mapping results. The crystal phases and crystallinity of the $CoMoO_4$ NWAs were examined by XRD. The results demonstrate the monoclinic $CoMoO_4$ (PDF card, No. 21-0868). Additionally, several weak diffraction peaks attributed to $CoMoO_4{\cdot}9H_2O$ are found. The results are consistent with the previous reports [3, 9]. Figure 2c, d exhibits the TEM

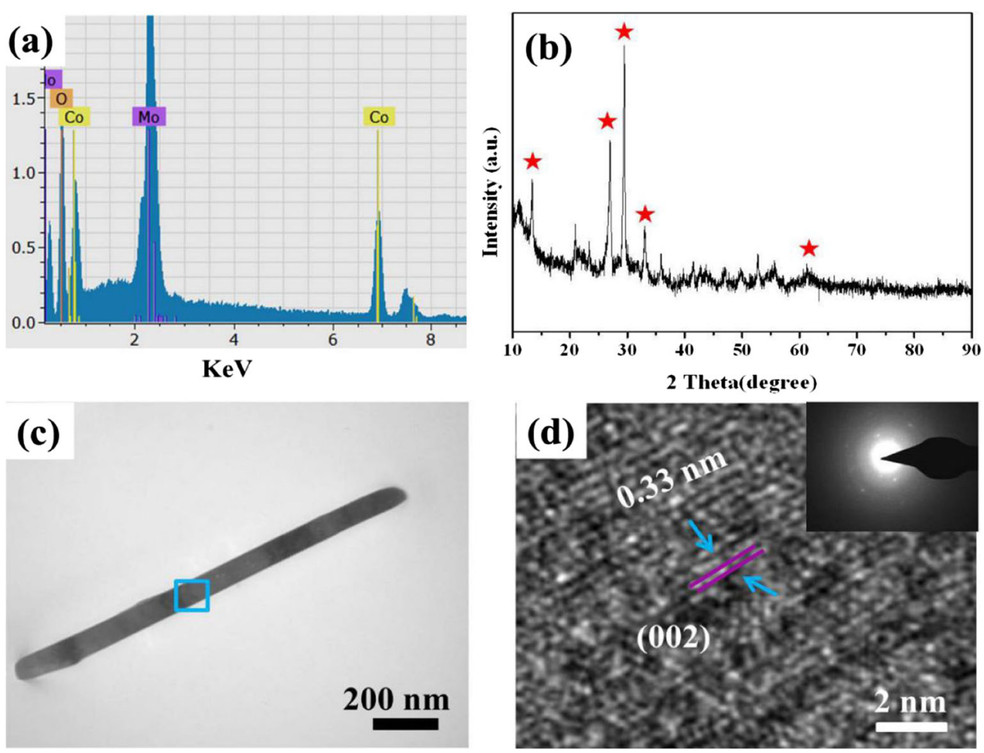


**Fig. 2** **a** The EDS spectrum of $CoMoO_4$ NWAs. **b** XRD pattern of $CoMoO_4$ NWAs. **c** TEM image of an individual $CoMoO_4$ NWAs. **d** HRTEM image of the as-prepared $CoMoO_4$ NWAs and the inset is the corresponding SAED pattern

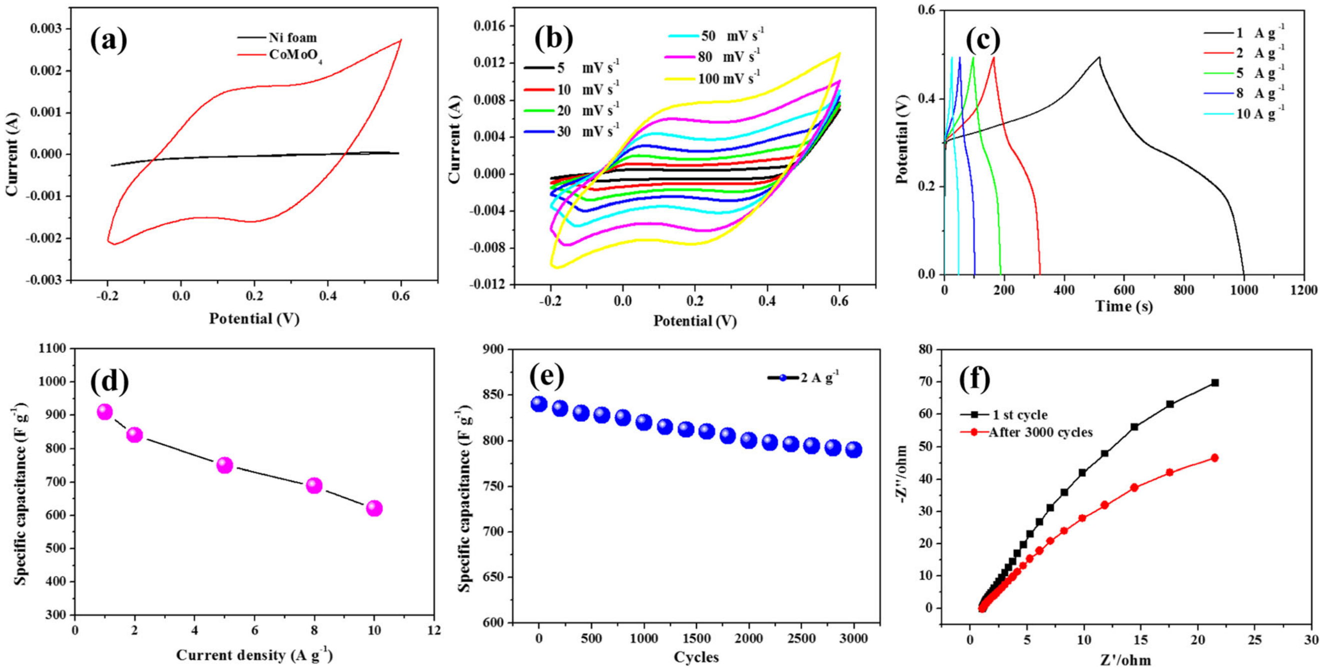


**Fig. 3** **a** CV curves of the Ni foam and $CoMoO_4$ NWAs. **b** CV curves of $CoMoO_4$ NWAs at different scan rates. **c** Charge-discharge curves of $CoMoO_4$ NWAs at different current densities. **d** Specific capacitance of $CoMoO_4$ NWAs at varied current densities. **e** The cycling performance of $CoMoO_4$ NWAs at the current density of 2 A $g^{-1}$. **f** Nyquist plot of $CoMoO_4$ NWAs

and HRTEM images of $CoMoO_4$ NWAs. The lattice fringes suggest the lattice spacing is 0.33 nm, which is corresponding to the (002) planes of $CoMoO_4$. The SEAD in Fig. 2d indicates the polycrystalline characteristics of $CoMoO_4$ NWAs.

The electrochemical performance of the $CoMoO_4$ NWAs on Ni substrate is evaluated in a three-electrode electrochemical cell with 2 M KOH aqueous solution. Figure 3a displays the CV curves of Ni foam and $CoMoO_4$ NWAs at the scan rate of 20 mV $s^{-1}$. The results revealed that the interconnected $CoMoO_4$ NWA electrode exhibits higher capacitive current density than that of Ni foam. Further confirmed, the pure Ni foam contributes little to the total capacitance of the $CoMoO_4$ NWA electrode. Figure 3b exhibits the CV curves of $CoMoO_4$ NWAs at different scan rates. These CV curves indicate the pseudocapacitance features and the curves keep the original shape with the scan rate increasing, demonstrating of the fast ionic and electron transportation of the $CoMoO_4$ NWA electrode. The peak current increases with the increase of the scan rate, indicating the good reversibility during the fast charge-discharge process. Charge-discharge curves were further tested at different current densities as shown in Fig. 3c. The charge-discharge curves indicate good symmetry, revealing the desirable electrochemical reversibility and charge-discharge performance. The specific capacitances of the as-prepared products calculated according to Eq. (1) are 910, 840, 750, 688, and 620 F $g^{-1}$ at the current density of 1, 2, 5, 8, and 10 A $g^{-1}$,

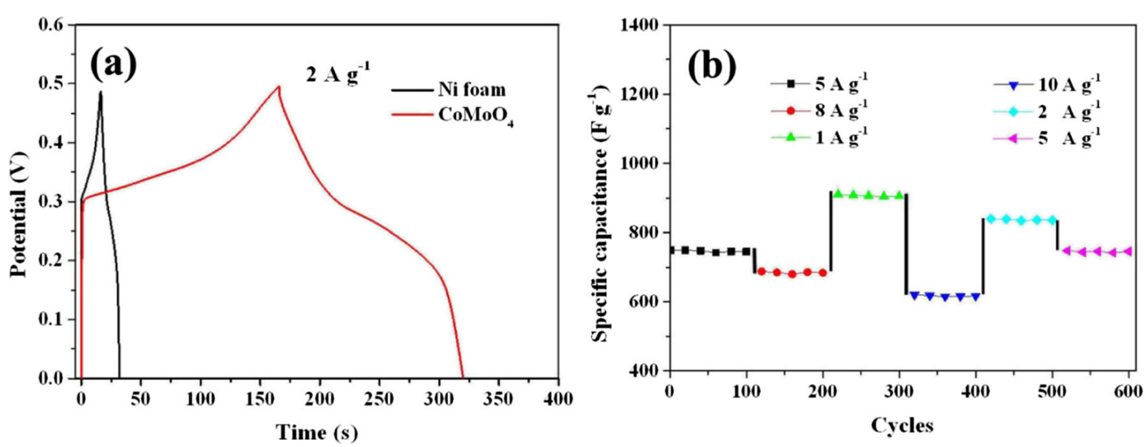


**Fig. 4** **a** Charge-discharge curves of the Ni foam and $CoMoO_4$ NWAs at the current density of 2 A $g^{-1}$. **b** Cycling stability of $CoMoO_4$ NWAs at different current densities

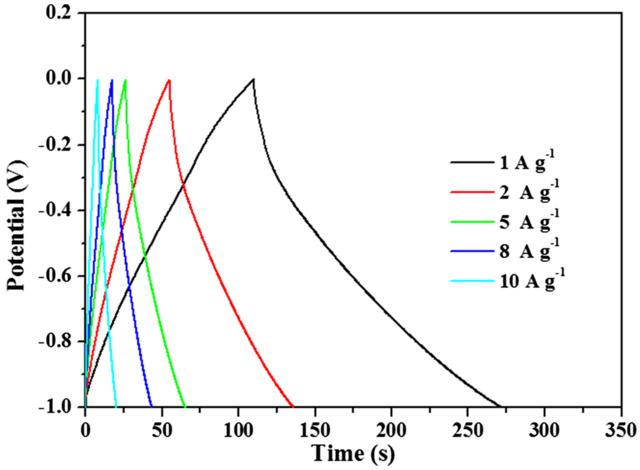


**Fig. 5** Charge-discharge curves of the AC electrode at different current densities

respectively (as shown in Fig. 3d). A charge-discharge cycling test was examined at the current density of 2 A $g^{-1}$ for 3000 cycles as shown in Fig. 3e. The specific capacitance of the $CoMoO_4$ NWA electrode changes from 840 to 790 F $g^{-1}$, which keeps 94% capacitance retention. The high specific capacitance and excellent cycling stability of the $CoMoO_4$ NWA electrode are impressive values when compared to those of many previously reported $CoMoO_4$ or $Co_3O_4$ oxide-based electrodes, as shown in Table S1. The Nyquist plots of the $CoMoO_4$ NWA electrode after the 1st and 3000th cycles are displayed in Fig. 3f. The arc increment is no obvious difference, indicating the structures are well maintained with little deformation. The slope of the curve illustrates the Warburg impedance is increased after 3000 cycles. It is attributed to the loss of some active materials during the charge-discharge process. Figure 4a presents the charge-discharge curves of Ni foam and $CoMoO_4$ NWAs at the current density of 2 A $g^{-1}$. Discharge time of Ni foam is less than 10 s. However, discharging time of $CoMoO_4$ NWAs is more than 150 s, demonstrating that the obtained product possesses an excellent charge-discharge performance.

Figure 4b presents the current density dependent cycling performance. At the first 100 cycles with the current density of 5 A $g^{-1}$, the specific capacitance is stable. After changing the current density continuously, the specific capacitance still keeps stable after returning to 5 A $g^{-1}$. These results indicate that the $CoMoO_4$ NWA electrode possesses good electrochemical performance. It can be concluded as follows: Firstly, the $CoMoO_4$ NWA electrode was directly grown on Ni substrate so that this electrode has better electrical conductivity. Secondly, the 1-dimensional nanowires connected with each other forming the network structure, which is easier for the electrolyte penetrating to the surface of the electrode. Thirdly, this nanostructure also shortens the diffusion path of the ions and electrons and accelerates the electrochemical reactions.

An ASC device was further assembled to explore the electrochemical performance. $CoMoO_4$ NWA electrode was used as cathode and AC on Ni foam as anode. Before assembling the device, the charge between the $CoMoO_4$ NWA cathodes

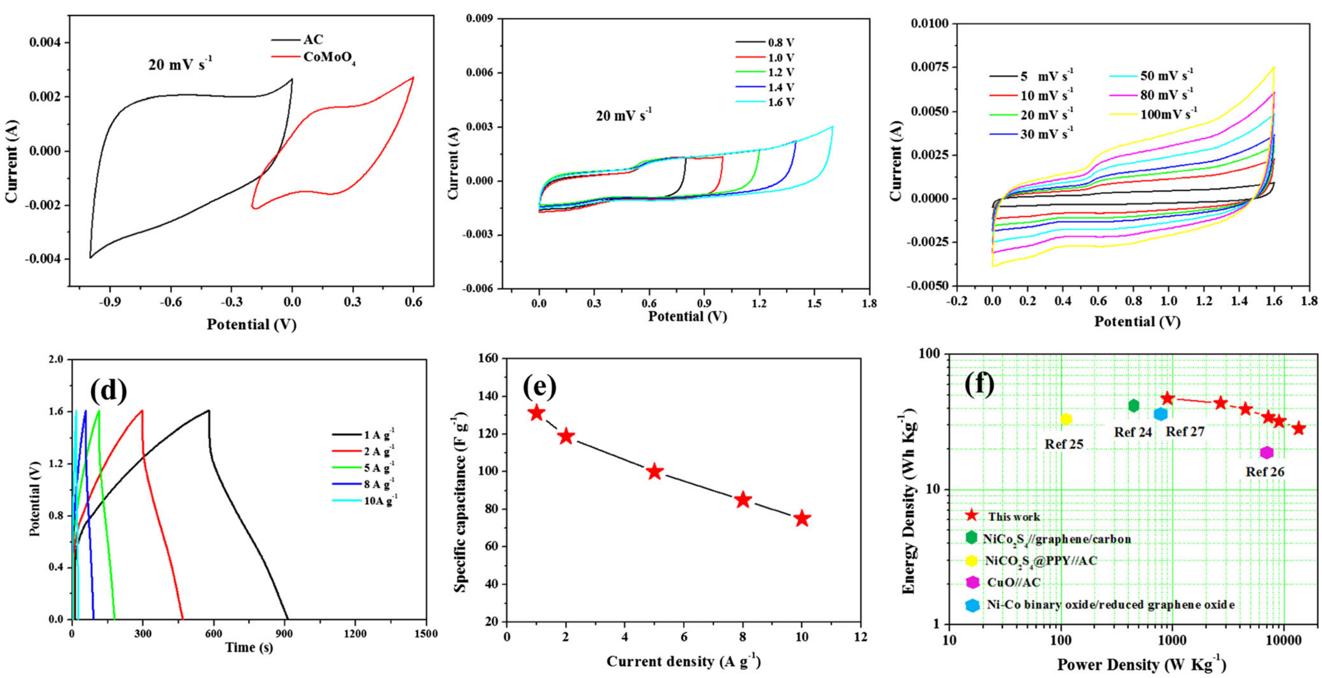


**Fig. 6** **a** CV curves of AC and $CoMoO_4$ NWA electrodes performed in a three-electrode cell in a 2 M KOH electrolyte at a scan rate of 20 mV $s^{-1}$. **b** CV curves of $CoMoO_4$//AC ACS device tested at different potential windows at the same scan rate of 20 mV $s^{-1}$. **c** CV curves of $CoMoO_4$//AC ACS device at different scan rates. **d** Charge-discharge curves of $CoMoO_4$//AC ACS device at different current densities. **e** Specific capacitance of $CoMoO_4$ NWAs at varied current densities. **f** Ragone plots relating power density to energy density of the $CoMoO_4$//AC ACS device

and the AC anode was optimized. The mass ratios for the two electrodes were calculated by the specific capacitance values and potential windows. Figure 5 demonstrates the charge-discharge curves of AC with a potential window of − 1 to 0 V at different current densities.

The charge and the optimal mass ratio between the $CoMoO_4$ NWA cathode and the AC anode are calculated to be 1:3 according to the specific capacitance values and potential windows. Figure 6a exhibits the CV curves of $CoMoO_4$ NWAs//AC ASC device at the scan rate of 20 mV $s^{-1}$. The potential windows of the AC and $CoMoO_4$ NWA electrodes are − 1 to 0 and − 0.2 to 0.6 V, respectively.

Figure 6b shows the CV curves of $CoMoO_4$ NWAs//AC ASC device at different potential windows. These CV curves present nearly rectangular curves at different potential windows. The $CoMoO_4$ NWAs//AC ASC device can use the sum of the potential range for AC and $CoMoO_4$ NWA electrodes 1.6 V. Figure 6c reveals the CV curves of $CoMoO_4$ NWAs//AC ASC device at different scan rates. When the scan rate increased, these CV curves remain the same shape, indicating the fast charge-discharge of the ASC device. Charge-discharge tests were explored at different current densities as illustrated in Fig. 6d. Discharge curves were nearly symmetrical to the charge curves, suggesting good capacitive performance for the ASC device. The specific capacitances were calculated from the discharge curves of Fig.6d. The specific capacitances are 131.3, 118.8, 100, 85, and 75 F $g^{-1}$ at the current density of 1, 2, 5, 8, and 10 A $g^{-1}$ (as shown in Fig. 6e), respectively. Figure 6f demonstrates the Ragone plot of $CoMoO_4$ NWAs//AC ASC device. The energy density and power density of $CoMoO_4$ NWAs//AC ASC device were calculated according to Eqs. (2) and (3). The maximum energy density as high as 46.7 Wh $kg^{-1}$ is obtained at a current density of 1 A $g^{-1}$ with the power density of 800 W $kg^{-1}$ under the operating voltage of 1.6 V. This ASC device possesses a maximum of 8000 W $kg^{-1}$ power density at the current density of 10 A $g^{-1}$ with the energy density of 26.7 Wh $kg^{-1}$ with an operating potential of 1.6 V. We compared our work with the previous reported work as shown in Fig. 6f. It is clearly seen that the energy and power density of $CoMoO_4$ NWAs//AC ASC are larger than those of the as-reported $NiCo_2S_4$//grapheme/carbon [23], $NiCo_2S_4$@PPy//AC [24], CuO//AC [25], and Ni-Co binary oxide//reduced graphene oxide [26] due to the improved specific capacity and wide potential window from 0 to 1.6 V.

## Conclusion

In summary, $CoMoO_4$ nanowires were successfully fabricated by a simple hydrothermal method under the low temperature 90 °C. The $CoMoO_4$ nanowire electrode shows high specific capacitance 910 F $g^{-1}$ at the current density of 1 A $g^{-1}$ and good cycle performance 94% capacitance retention (at the current density of 2 A $g^{-1}$ for 3000 cycles). The $CoMoO_4$ NWAs//AC ASC indicates high energy density (46.7 Wh $kg^{-1}$ at a power density of 800 W $kg^{-1}$) and power density (8000 W $kg^{-1}$ at 26.7 Wh $kg^{-1}$), which is believed to be a promising energy storage device in the future.

**Funding information** This study was supported by the Foundation for Young Scientists of Harbin University of Commerce, No.17XN018.

## References

1. Simon P, Gogotsi Y (2008) Materials for electrochemical capacitors. Nat Mater 7:845–854
2. Yang PH, Ding Y, Lin ZY, Chen ZW, Li YZ, Qiang PF, Ebrahimi M, Mai WJ, Wong P, Wang ZL (2014) Low-cost high-performance solid-state asymmetric supercapacitors based on $MnO_2$ nanowires and $Fe_2O_3$ nanotubes. Nano Lett 14(2):731–736
3. Wang J, Liu SK, Zhang X, Liu XS, Liu XX, Li N, Zhao JP, Li Y (2016) A high energy asymmetric supercapacitor based on flower-like $CoMoO_4/MnO_2$ heterostructures and activated carbon. Electrochim Acta 13(20):663–671
4. Wei G, Xu XR, Liu JX, Du K, Du J, Zhang S, An CH, Zhang J, Wang ZJ (2017) Carbon quantum dots decorated hierarchical Ni $(OH)_2$ with lamellar structure for outstanding supercapacitor. Mater Lett 186(1):131–134
5. Fu K, Li YP, Dirican M, Chen C, Lu Y, Zhu JD, Li Y, Cao LY, Bradford PD, Zhang XW (2014) Sulfur gradient-distributed CNF composite: a self-inhibiting cathode for binder-free lithium-sulfur batteries. Chem Commun 50(71):10277–10280
6. Tong ZQ, Yang YN, Wang JY, Zhao JP, Su BL, Li Y (2014) Layered polyaniline/graphene film from sandwich-structured polyaniline/graphene/polyaniline nanosheets for high-performance pseudosupercapacitors. J Mater Chem A 2(13):4642–4651
7. Wang S, Sun SM, Li SD, Gong FL, Li YN, Wu Q, Song P, Fang SM, Wang PY (2016) Time and temperature dependent multiple hierarchical $NiCo_2O_4$ for high-performance supercapacitors. Dalton Trans 45(17):7469–7475
8. Sun SM, Wang S, Li SD, Li YN, Zhang YH, Chen JL, Zhang ZH, Fang SM, Wang PY (2016) Asymmetric supercapacitors based on a $NiCo_2O_4$/three dimensional graphene composite and three dimensional graphene with high energy density. J Mater Chem A 4(47): 18646–18653
9. Wang J, Zhang X, Wei QL, Lv HM, Tian YL, Tong ZQ, Liu XS, Hao J, Qu HY, Zhao JP, Li Y, Mai LQ (2016) 3D self-supported nanopine forest-like $Co_3O_4$@$CoMoO_4$core-shell architectures for high-energy solid state supercapacitors. Nano Energy 19:222–233
10. Su YZ, Xiao K, Li N, Liu ZQ, Qiao SZ (2014) Amorphous $Ni(OH)_2$ @ three-dimensional Ni core–shell nanostructures for high capacitance pseudocapacitors and asymmetric supercapacitors. J Mater Chem A 2(34):13845–13583
11. Demarconnay L, Raymundo-Piñero E, Béguin E (2011) Adjustment of electrodes potential window in an asymmetric carbon/$MnO_2$ supercapacitor. J Power Sources 196(1):580–586
12. Xu YN, Wang XF, An CH, Wang YJ, Jiao LF, Yuan HT (2014) Facile synthesis route of porous $MnCo_2O_4$ and $CoMn_2O_4$ nanowires and their excellent electrochemical properties in supercapacitors. J Mater Chem A 2:16480–16488
13. Yu GH, Hu LB, Vosgueritchian M, Wang HL, Xie X, McDonough JR, Cui X, Cui Y, Bao ZN (2011) Solution-processed graphene/ $MnO_2$ nanostructured textiles for high-performance electrochemical capacitors. Nano Lett 11(7):2905–2911

14. Huang G, Zhang LL, Zhang FF, Wang LM (2014) Metal-organic framework derived $Fe_2O_3$@$NiCo_2O_4$ porous nanocages as anode materials for Li-ion batteries. Nano 6(10):5509–5515
15. Zhu YG, Wang Y, Shi Y (2014) Phase transformation induced capacitance activation for 3D graphene-CoO nanorod pseudocapacitor. Adv Energy Mater 4(9):1301788
16. Zhang Z, Liu YD, Huang ZY, Ren L, Qi X, Wei XL, Zhang JX (2015) Facile hydrothermal synthesis of $NiMoO_4$@$CoMoO_4$ hierarchical nanospheres for supercapacitor applications. Phys Chem Chem Phys 17:20795–20804
17. He D, Xing SX, Sun BN, Cai H, Suo H, Zhao C (2016) Design and construction of three-dimensional flower-like CuO hierarchical nanostructures on copper foam for high performance supercapacitor. Electrochim Acta 210(20):639–645
18. Cao F, Pan GX, Tang PS, Chen HF (2012) Hydrothermal-synthesized $Co(OH)_2$ nanocone arrays for supercapacitor application. J Power Sources 216(15):395–399
19. Peng SJ, Li LL, Wu HB, Madhavi S, Lou XW (2015) Controlled growth of $NiMoO_4$ nanosheet and nanorod arrays on various conductive substrates as advanced electrodes for asymmetric supercapacitors. Adv Energy Mater 5(2):1401172
20. Yang Q, Lu ZY, Sun XM, Liu JF (2013) Ultrathin $Co_3O_4$ nanosheet arrays with high supercapacitive performance. Sci Rep 3:3537–3544
21. Li S, Li X, Liu J, Shang Z, Cui X (2014) A low-temperature electrolyte for lithium-ion batteries. Ionics 21(4):901–907
22. Liu MC, Kong LB, Lu C, Li XM, Luo YC, Kang L (2013) Facile fabrication of $CoMoO_4$ nanorods as electrode material for electrochemical capacitors. Mater Lett 94(1):197–200
23. Shen LF, Yu L, Wu HB, Yu XY, Zhang XG, Lou XW (2015) Formation of nickel cobalt sulfide ball-in-ball hollow spheres with enhanced electrochemical pseudocapacitive properties. Nat Commun 6:1–8
24. Yan ML, Yao YD, Wen JQ, Long L, Kong ML, Zhang GG, Liao XM, Yin GF, Huang ZB (2016) Construction of a hierarchical $NiCo_2S_4$@PPy core-shell heterostructure nanotube array on Ni foam for a high-performance asymmetric supercapacitor. ACS Appl Mater Interfaces 8(37):24525–24535
25. Moosavifard SE, El-Kady MF, Rahmanifar MS, Kaner RB, Mousavi MF (2015) Designing 3D highly ordered nanoporous CuO electrodes for high-performance asymmetric supercapacitors. CS Appl Mater Interfaces 7(8):4851–4860
26. Bai Y, Liu MM, Sun J, Gao L (2016) Fabrication of Ni-Co binary oxide/reduced graphene oxide composite with high capacitance and cyclicity as efficient electrode for supercapacitors. Ionics 22(4): 535–544